



Contents lists available at ScienceDirect

Journal of the Mechanical Behavior of Biomedical Materials

journal homepage: [www.elsevier.com/locate/jmbbm](http://www.elsevier.com/locate/jmbbm)

# Impact of the sintering parameters on the grain size, crystal phases, translucency, biaxial flexural strength, and fracture load of zirconia materials

Felicitas Mayinger<sup>a,\*</sup>, Andreas Ender<sup>b</sup>, Monika Strickstroch<sup>c</sup>, Adham Elsayed<sup>a</sup>, Parissa Nassary Zadeh<sup>a</sup>, Marcus Zimmermann<sup>b</sup>, Bogna Stawarczyk<sup>a</sup>

<sup>a</sup> Department of Prosthetic Dentistry, University Hospital, LMU Munich, Goethestraße 70, 80336, Munich, Germany

<sup>b</sup> Division of Computerized Restorative Dentistry, Clinic of Conservative and Preventive Dentistry, Center of Dental Medicine, University of Zurich, Plattenstrasse 11, 8032, Zurich, Switzerland

<sup>c</sup> Faculty of Engineering and Computer Science, Material Science and Analysis, University of Applied Sciences Osnabrück, Albrechtstraße 30, 49076, Osnabrück, Germany

## ARTICLE INFO

### Keywords:

Zirconia  
High-speed sintering  
Speed-sintering

## ABSTRACT

**Objectives:** To investigate the influence of the zirconia and sintering parameters on the optical and mechanical properties.

**Methods:** Three zirconia materials (3/4Y-TZP, 4Y-TZP, 3Y-TZP) were high-speed (HSS), speed (SS) or conventionally (CS) sintered. Disc-shaped specimens nested in 4 vertical layers of the blank were examined for grain size (GS), crystal phases (c/t'/t/m-phase), translucency (T), and biaxial flexural strength. Fracture load (FL) of three-unit fixed dental prostheses was determined initially and after thermomechanical aging. Fracture types were classified, and data statistically analyzed.

**Results:** 4Y-TZP showed a higher amount of c + t'-phase and lower amount of t-phase, and higher optical and lower mechanical properties than 3Y-TZP. In all materials, T declined from Layer 1 to 4. 3/4Y-TZP showed the highest FL, followed by 3Y-TZP, while 4Y-TZP showed the lowest. In 4Y-TZP, the sintering parameters exercised a direct impact on GS and T, while mechanical properties were largely unaffected. The sintering parameters showed a varying influence on 3Y-TZP. Thermomechanical aging resulted in comparable or higher FL.

**Conclusion:** 3/4Y-TZP presenting the highest FL underscores the principle of using strength-gradient multi-layer blanks to profit from high optical properties in the incisal area, while ensuring high mechanical properties in the lower areas subject to tensile forces. With all groups exceeding maximum bite forces, the examined three-unit FDPs showed promising long-term mechanical properties.

## 1. Introduction

The first zirconia materials, made of 3 mol% yttria stabilized-tetragonal zirconia polycrystal (3Y-TZP), captivated the dental market with their mechanical prowess (Stawarczyk et al., 2012). A reallocation of the alumina particles to the grain boundaries, paired with a decrease in the total amount of alumina from 0.25 to 0.05 wt%, led to a desired improvement of the optical properties (Stawarczyk et al., 2016; Zhang et al., 2016). The further pursuit of this aim culminated in the development of zirconia with an increased amount of yttrium oxide (5Y-TZP). The high esthetic properties of this group did, however, come at the cost of notably reduced mechanical properties (flexural strength: ~500 MPa)

(Zhang et al., 2016; Nassary Zadeh et al., 2018), challenging the central competitive edge of zirconia materials in comparison with highly esthetic silicate-based ceramics. This was met by introducing 4Y-TZP, an all-rounder that aims to merge optical and mechanical properties (Jansen et al., 2019; Jerman et al., 2021; Rosentritt et al., 2020). Based on x-ray diffraction (XRD) analyses, the crystal phases of zirconia can be categorized, i.e., as cubic (c-phase), tetragonal-prime (t'-phase), tetragonal (t-phase), or monoclinic (m-phase) (Wertz et al., 2021; Belli et al., 2021). While 3Y-TZP materials are characterized by their ability to undergo tetragonal to monoclinic phase transformations that entail a volumetric expansion of 3–5% and account for the materials' high fracture toughness (Hannink and Muddle, 2000), an increase of the

\* Corresponding author. Department of Prosthetic Dentistry Dental School, University Hospital, LMU Munich, Goethestrasse 70, 80336, Munich, Germany.  
E-mail address: [felicitas.mayinger@med.uni-muenchen.de](mailto:felicitas.mayinger@med.uni-muenchen.de) (F. Mayinger).

<https://doi.org/10.1016/j.jmbbm.2024.106580>

Received 12 March 2024; Received in revised form 6 May 2024; Accepted 10 May 2024

Available online 14 May 2024

1751-6161/© 2024 Published by Elsevier Ltd. This is an open access article under the CC BY license (<http://creativecommons.org/licenses/by/4.0/>).

yttrium oxide content and in consequence an increase of crystal phases with a tetragonality approximating 1.000 introduced fully stabilized zirconia (Zhang et al., 2016; Camposilvan et al., 2018). With the  $t'$ - and  $c$ -phase being non-transformable, materials with an yttrium oxide content  $\geq 5$  mol% are insusceptible to hydrothermal aging (Zhang et al., 2016; Camposilvan et al., 2018). The latest trend in the development of zirconia are multi-layer blanks (e.g., KATANA Zirconia YML that incorporates 4 different vertical layers), that impersonate the varying esthetic appearance of natural teeth, from their translucent and brighter incisal edge to the more opaque and darker body. This gradient can either be achieved by an incremental dotting with pigments (color-gradient blanks) or the incorporation of different zirconia compositions in one blank (strength-gradient blanks) (Michailova et al., 2020; Kolkarnprasert et al., 2019).

To allow an optimal integration of the manufacturing of such zirconia restorations into the digital chairside workflow, time is of the essence. Against this background, speed (SS) and high-speed sintering (HSS) protocols have been developed. These protocols work with a reduced holding time, which is compensated by an increased heating rate and firing temperature. A variation of these sintering parameters does, however, affect the properties of the zirconia (Jansen et al., 2019; Jerman et al., 2020; Kaizer et al., 2017; Liu et al., 2022a). In this context, the area under the curve (AUC) above a sintering temperature of 1200 °C in a time-temperature graph of sintering protocols is decisive. A larger AUC, a higher firing temperature and longer sintering durations are linked to an increased grain size (GS) (Stawarczyk et al., 2014). An increase in GS entails an increase in the translucency of the zirconia, while simultaneously resulting in decreased mechanical properties above a sintering temperature of 1550 °C due to grain growth and the formation of voids (Stawarczyk et al., 2013). To the authors' best knowledge, the consequences of varying sintering parameters on the properties of 4Y-TZP and strength-gradient multi-layer compositions have not been conclusively examined (Jansen et al., 2019; Rosentritt et al., 2022; Liu et al., 2022b).

The aim of this investigation was to examine the influence of different zirconia (3/4Y-TZP, 4Y-TZP, 3Y-TZP) and sintering parameters on the GS, crystal phases, translucency ( $T$ ), and biaxial flexural strength ( $BFS$ ) of the zirconia in 4 different layers and the fracture load ( $FL$ ) of three-unit fixed dental prostheses (FDPs) initially and after

thermomechanical aging.

The first hypothesis stated that neither the zirconia material, layer nor the sintering protocol present an impact on the GS, crystal phases,  $T$ , and  $BFS$ . The second hypothesis stated that neither the zirconia material, the sintering protocol nor thermomechanical aging influence the  $FL$  of the three-unit FDPs.

## 2. Materials and methods

The GS, crystal phases,  $T$ , and  $BFS$  in 4 different vertical layers and the  $FL$  of three-unit FDPs initially and after thermomechanical aging of 3 zirconia materials (KATANA Zirconia YML, 3/4Y-TZP (Lot No: AT1001, EESGR), KATANA Zirconia STML, 4Y-TZP (Lot No: EDEUI) and KATANA Zirconia HTML, 3Y-TZP (Lot No: ECVXI), Kuraray Noritake Dental, Tokyo, Japan) sintered according to 3 or 2 different sintering protocols were examined (Fig. 1).

### 2.1. Specimen preparation

Nesting in the 4 layers of the zirconia blanks ( $\phi$  98.5 x 14 mm) was performed using inLab CAM (v.20.0.1; Dentsply Sirona, Konstanz, Germany) (Fig. 2., Appendix Fig. A1.).

Disc-shaped specimens were designed as cylinders with a height of 1.5 mm and a diameter of 16 mm. For the three-unit FDPs spanning from the first premolar to the first molar, a master STL file with a cross-sectional area of 9 mm<sup>2</sup> in the connectors was used (S2). To ensure a three-point contact during thermomechanical aging and fracture loading, the pontics were designed with a central cavity.

Disc-shaped specimens and three-unit FDPs were milled (inLab MC X5, Dentsply Sirona) and separated from the presintered zirconia blanks with a diamond bur. Each specimen was carefully cleaned to remove surplus milling dust.

3/4Y-TZP and 4Y-TZP were sintered using a high-speed sintering, a speed sintering or a conventional sintering protocol. 3Y-TZP was sintered using a speed sintering or conventional sintering protocol. All subgroups except for the high-speed sintered 4Y-TZP, which was fired using CEREC SpeedFire (Dentsply Sirona), were fired using inLab Profire (Dentsply Sirona). The different heating rates up to a specified temperature, the firing temperature and respective holding time, the cooling

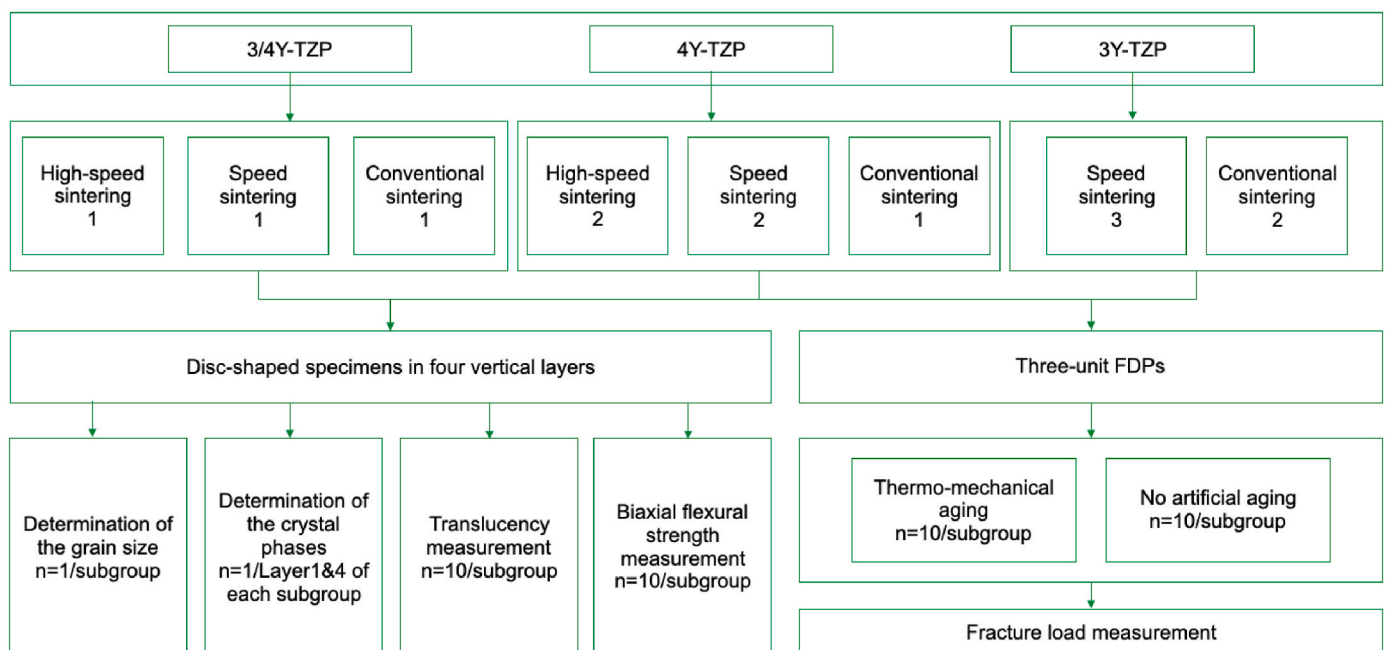


Fig. 1. Study design.

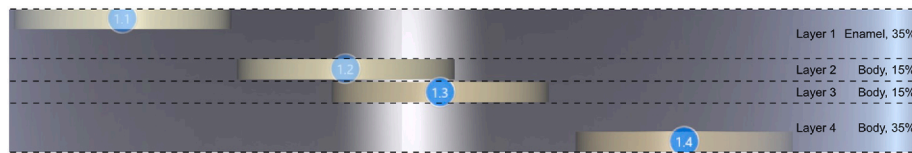


Fig. 2. Nesting of the disc-shaped specimens in the 4 layers of the zirconia blank (from Layer 1 at the top to Layer 4 at the bottom of the blank).

rate to a specified temperature and the overall duration of the different sintering protocols are shown in Table 1.

After sintering, disc-shaped specimens were ground from both sides (Abramin, Struers, Ballerup, Denmark) with 2 diamond pads (MD-Piano 220 and MD-Piano 500, Struers) and polished to 9 μm using a diamond suspension (DP-Suspension M, Struers) on a polishing pad (MD-Largo and MD-Chem, Struers). The final thickness of 1.2 ± 0.01 mm was verified with a digital micrometer screw with an accuracy of ±4 μm (IP65, Mitutoyo, Kawasaki, Japan).

### 2.2. Determination of the grain size

Specimens were thermally etched at 1450 °C for 30 min (LHT 02/16, Nabetherm, Lillienthal, Germany). The top surface of each specimen was sputtered with gold and surface topography was examined with a scanning electron microscope (SEM; GeminiSEM 450, Zeiss, Oberkochen, Germany) working with 10 kV at a distance of 5.0 mm. The grain sizes were visually analyzed and described.

### 2.3. Determination of the crystal phases

XRD patterns in Layers 1&4 were obtained using a Bragg Brentano diffractometer (D8 Advance, Bruker AXS, Karlsruhe, Germany) with CuKα radiation (40 mA, 40 kV) and a Lynx-eye detector (1D mode) within the range of 20–120° 2θ (step size 0.02°, 2 s/step). Rietveld refinement was performed using Topas64 V6 (Bruker AXS). Background fitting used Chebychev polynomials and peak profiles were fitted with fundamental parameters. Crystal structures were taken from the Inorganic Crystal Structure Database (ICSD) (ICSD codes: tetragonal 75311, cubic 75316 and monoclinic 82543). Based on best fit, crystal phases were defined as t, t', c or m. The tetragonal phases differed by the tetragonality factor t': 1.005–1.006 and t: 1.015–1.017. For the graphical output (EVA V4.2.2.), the Kα was subtracted from the scan with a value of 0.5.

Table 1  
Sintering protocols for the different materials.

Material	Sintering protocol	Abbreviation	Oven	Heating rate 1	T1	Heating rate 2	T2	Heating rate 3	T3	Firing temperature	Holding time	Cooling rate	T4	Duration
				°C/min	°C	°C/min	°C	°C/min	°C	°C	min	°C/min	°C	h:min
3/4Y-TZP	High-speed sintering 1	HSS 1	inLab Profire	120	1450	10	1600	–	–	1600	20	120	800	00:54
	Speed sintering 1	SS 1	inLab Profire	50	1400	4	1500	10	1560	1560	16	50	800	1:30
	Conventional sintering 1 <sup>a</sup>	CS 1	inLab Profire	10	1550	–	–	–	1550	120	10	RT	7:05	
4Y-TZP	High-speed sintering 2	HSS 2	CEREC Speed Fire	130	900	50	1500	15	1560	1560	16	70	800	00:50
	Speed sintering 2	SS 2	inLab Profire	35	1560	–	–	–	1560	30	45	RT	1:48	
	Conventional sintering 1 <sup>a</sup>	CS 1	inLab Profire	10	1550	–	–	–	1550	120	10	RT	7:05	
3Y-TZP	Speed sintering 3	SS 3	inLab Profire	35	1515	–	–	–	1515	30	45	RT	1:46	
	Conventional sintering 2	CS 2	inLab Profire	10	1500	–	–	–	1500	120	10	RT	6:55	

<sup>a</sup> Identical sintering protocols; RT: Room temperature; T: temperature.

### 2.4. Translucency measurement

The *T* was determined with a spectrophotometer (CM-26dG, Konica Minolta, Hannover, Germany) using the CIE illuminant D65 as a light source. Each specimen was measured 3 times in front of a white (*Y<sub>w</sub>*) and black (*Y<sub>b</sub>*) background using the flashing mode. Mean values were directly calculated within the software. The *T* was determined from the luminous reflectance (*Y*) with the following equation:

$$T = 100 - Y_b / Y_w$$

where *T* is the translucency [%] and *Y<sub>b</sub>* is the luminous reflectance over a black and *Y<sub>w</sub>* the luminous reflectance over a white background, with *Y* equal to:

$$Y = [(L^* + 16) / 116]^3 Y_n$$

where *L\** is the lightness and *Y<sub>n</sub>* the reference illuminant.

A value of 0 was considered as opaque and a value of 1 as transparent.

### 2.5. Biaxial flexural strength measurement

*BFS* was determined in a universal testing machine (Zwick 1445, ZwickRoell, Ulm, Germany) equipped with a plunger (diameter of 1.6 mm) moving at a crosshead speed of 1 mm/min. Specimens were placed on 3 balls (diameter of 3.2 mm) forming an equilateral triangle (Fig. A2). Loading was performed until failure occurred. *BFS* (*σ*) was calculated with the following equation (Technical Committee ISO/TC 106/SC 2 and International Organization for Standardization, 2015):

$$\sigma = - 0,2387 P (X - Y) / b^2$$

where *σ* is the maximum tensile stress [MPa], *P* is the fracture load [N], *b* is the specimen thickness [mm], and the coefficients *X* and *Y* equal:

$$X = (1 + \nu) \ln (r_2 / r_3)^2 + [(1 - \nu) / 2] (r_2 / r_3)^2 \text{ and}$$

$$Y = (1 + \nu) [1 + \ln(r_1 / r_3)^2] + (1 - \nu) (r_1 / r_3)^2$$

where  $\nu$  is Poisson's ratio ( $\nu = 0.3$ ),  $r_1$  is the radius of the support circle [mm],  $r_2$  is the radius of the loaded area [mm], and  $r_3$  is the specimen radius [mm].

Fracture types were classified by the number of radial cracks.

## 2.6. Fracture load measurement

Each FDP was bonded to a steel model imitating a prepared first premolar and first molar (diameter of respectively 7 mm or 8 mm, circular shoulder of 1 mm and taper of 6°), with a plastic covering of each abutment posing as the periodontal ligament (Rosentritt et al., 2011), using CLEARFIL CERAMIC PRIMER PLUS and PANAVIA V5 (Kuraray Noritake Dental), and stored in 37 °C deionized water (HERAcCell 150, Thermo Fisher Scientific, Waltham, USA) for 24 h. Half of the specimens underwent thermomechanical aging (Chewing Simulator CS-4.10, SD Mechatronik, Feldkirchen-Westerham, Germany; mechanical cycles: 1, 200,000, load: 50 N, frequency: 1.5 Hz; thermal cycles: 6,000, temperatures: 5 °C/55 °C, dwelling time: 60 s) opposed to steatite antagonists (steatite ball 1197, SD Mechatronik). The *FL* was determined employing the universal testing machine (Zwick 1445) operating at a crosshead

speed of 1 mm/min (Fig. A3). The measurement was aborted as soon as the maximum *FL* dropped by 20%. To avoid force peaks, a 0.1 mm tin foil (Dentaurum, Ispringen, Germany) was positioned between the specimens and the chrome-nickel steel testing stamp (diameter of 6 mm; SD Mechatronik). Fractures were documented with light microscope images taken at a magnification of 20x–500x (Keyence VHX-970F).

## 2.7. Statistical analyses

Data were descriptively analyzed. The Shapiro–Wilk test was employed to test for violations of the normal distribution. Significant differences between groups were analyzed with t-tests and one-way analyses of variance followed by post-hoc Scheffé test. Pearson's correlations were computed to test for correlations between the thickness, surface roughness, the amount of crystal phases, *T*, *BFS*, *FL* and the observed fracture types. All *P*-values below 0.05 were considered as statistically significant (IBM Statistics SPSS 26.0, IBM, Amonk, USA). Weibull moduli (*m*) were calculated for *BFS* and *FL* using the maximum likelihood estimation method at a 95% confidence level (Butikofer et al., 2015).

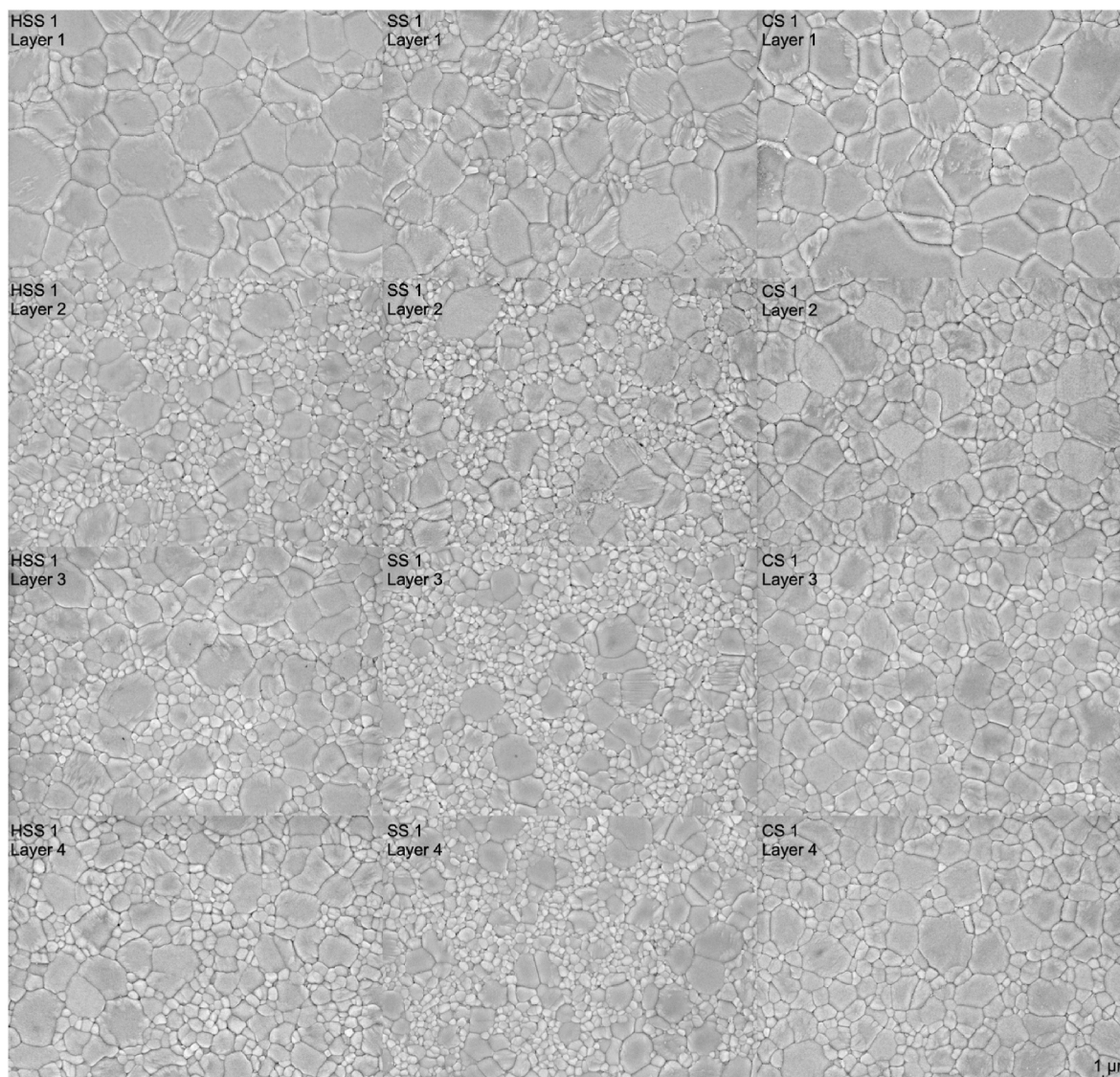


Fig. 3. (a–c). Scanning electron microscope images for each group (a. 3/4Y-TZP, b. 4Y-TZP, c. 3Y-TZP), taken at a 20'000x magnification.

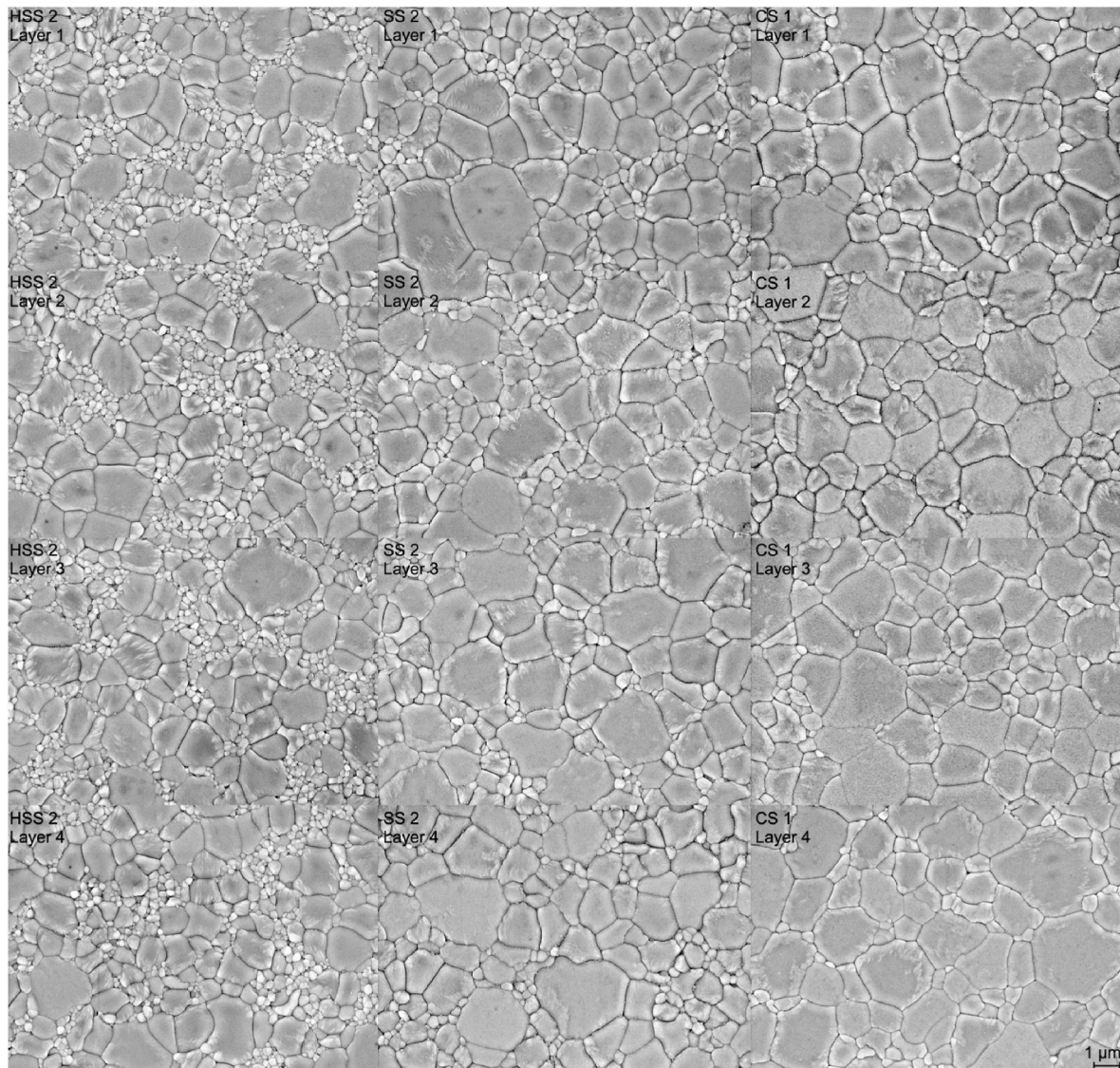


Fig. 3. (continued).

### 3. Results

With 3 of the 32 groups examined for translucency and biaxial flexural strength and 0 of 16 groups examined for fracture load showing a deviation from the normal distribution, data were analyzed parametrically.

#### 3.1. Grain size

##### 3.1.1. Influence of the zirconia and layer on the grain size

3/4Y-TZP – Layer 1 showed a comparable GS to 4Y-TZP, while 3/4Y-TZP Layers 2–4 presented smaller GSs like those seen for 3Y-TZP (Fig. 3).

##### 3.1.2. Influence of the sintering protocol on the grain size

In 3/4Y-TZP – Layer 1, HSS and conventional sintering (CS) led to a larger GS than seen after SS. In Layer 2, CS resulted in larger grains than observed following HSS or SS. In Layers 3&4, CS led to the largest GS, followed by HSS, while SS resulted in the smallest GS.

In 4Y-TZP, CS led to the highest homogeneity of the zirconia structure and the largest GS, followed by SS, while HSS showed an irregular distribution of smaller and larger grains.

In 3Y-TZP, CS resulted in the formation of larger grains in

comparison with SS.

#### 3.2. Crystal phases

##### 3.2.1. Influence of the zirconia on the crystal phases

3/4Y-TZP – Layer 1 and 4Y-TZP showed a higher amount of c- and t'-phase and a lower amount of t-phase than 3/4Y-TZP – Layer 4 and 3Y-TZP ( $p < 0.001$ ).

In 3/4Y-TZP – Layer 1 and 4Y-TZP the amount of c + t'-phase ranged from 73 to 84% and t-phase was <30%, while 3/4Y-TZP – Layer 4 and 3Y-TZP presented 42–53% c + t'-phase and 40–54% t-phase. The amount of m-phase ranged from 0 to 7% (Table 2).

##### 3.2.2. Influence of the zirconia layer on the crystal phases

In all materials except for conventionally sintered 3Y-TZP, Layer 1 showed a higher amount of c-phase than Layer 4.

##### 3.2.3. Influence of the sintering protocol on the crystal phases

Except for 3Y-TZP, that showed a decrease in the c-phase with an increasing sintering temperature, specimens showed a trend towards a decreasing amount of the t-phase and an increasing amount of c- and t'-phase with an increasing firing temperature.

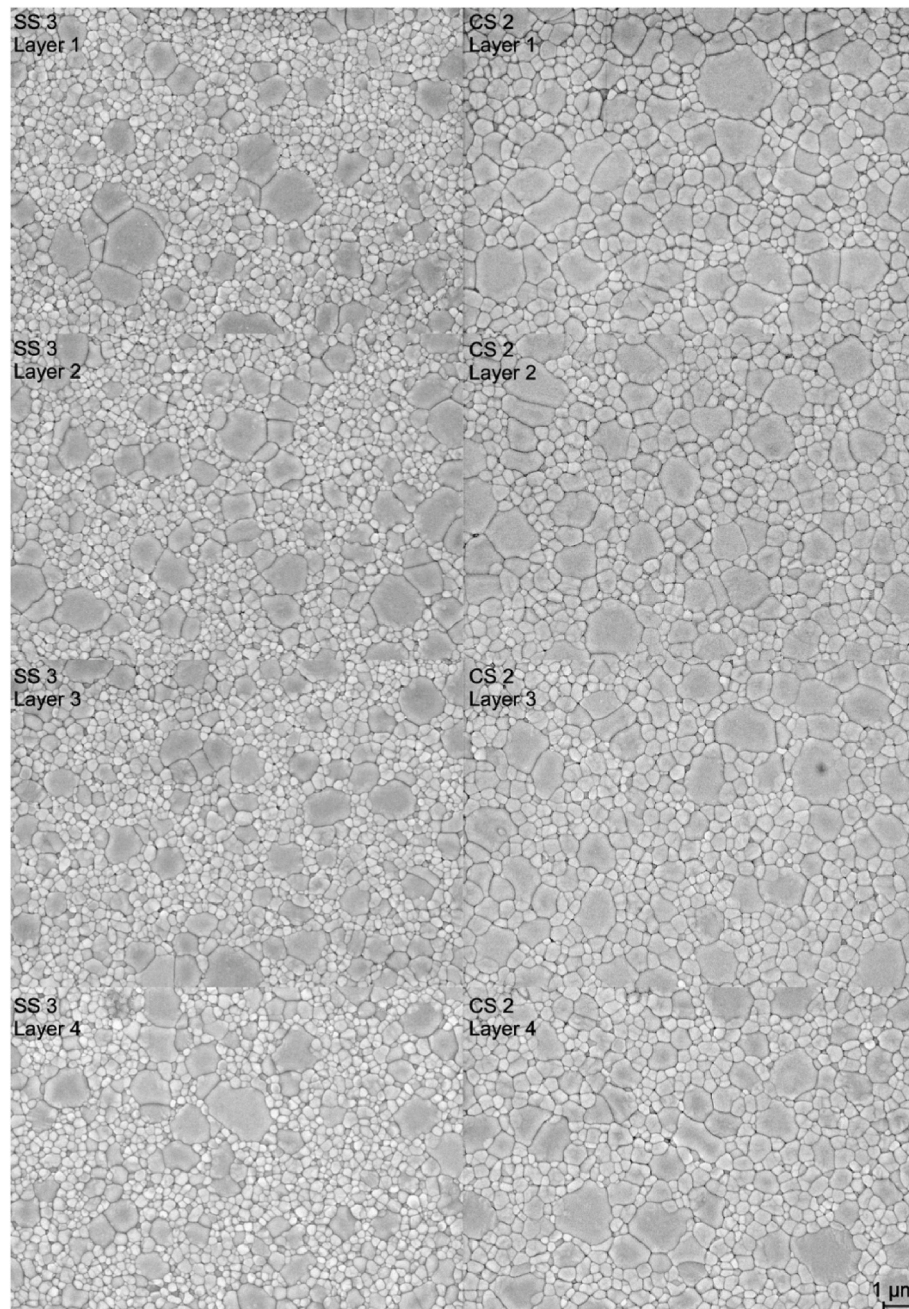


Fig. 3. (continued).

### 3.3. Translucency

#### 3.3.1. Influence of the zirconia on the translucency

When comparing all groups, the following trend could be observed: the highest  $T$  values were observed for 3/4Y-TZP – Layer 1, followed by the different 4Y-TZP Layers (Fig. 4).

The lower Layers of 3/4Y-TZP and 3Y-TZP behaved similarly, each showing a decline in  $T$  linked to the zirconia layer. In detail, 3/4Y-TZP – Layer 1, SS and CS 4Y-TZP – Layer 1 and CS 4Y-TZP - Layer 2 showed a higher  $T$  than all other groups, followed by the different 4Y-TZP groups and HSS and CS 3/4Y-TZP – Layer 2 ( $p < 0.001$ ). HSS 4Y-TZP – Layers 3 and 4 presented an exception and showed values that were in a similar value range as the different 3/4 and 3Y-TZP groups.

Following CS 1, 3/4Y-TZP showed a higher  $T$  in Layer 1, but lower values in Layers 2–4 than 4Y-TZP ( $p < 0.001$ ).

#### 3.3.2. Influence of the zirconia layer on the translucency

In all materials,  $T$  declined from Layer 1 (most translucent) to Layer 4 (least translucent) ( $p < 0.001$ ).

#### 3.3.3. Influence of the sintering protocol on the translucency

In 3/4Y-TZP – Layers 1, 3 and 4, CS resulted in the highest  $T$ , followed by HSS, while SS led to the lowest values ( $p < 0.001$ ). In 3/4Y-TZP – Layer 2, HSS and CS resulted in higher  $T$  values than SS ( $p < 0.001$ ).

In 4Y-TZP, CS resulted in the highest  $T$ , followed by SS, while HSS led to the lowest values ( $p < 0.001$ ).

In 3Y-TZP – Layers 1–3, CS resulted in a higher  $T$  than SS ( $p < 0.001$ ).

**Table 2**  
T', t, c, and m-phases [%] in the different groups (n = 1/each subgroup).

	Layer 1	Layer 4	Layer 1	Layer 4	Layer 1	Layer 4
3/4Y-TZP	HSS 1		SS 1		CS 1	
t' (%)	57	42	57	38	57	38
t (%)	16	48	17	40	24	54
c (%)	26	8	25	15	19	6
m (%)	1	2	1	7	0	2
4Y-TZP	HSS 2		SS 2		CS 1	
t' (%)	53	60	47	48	53	58
t (%)	14	17	24	27	19	23
c (%)	31	21	28	25	27	17
m (%)	2	2	1	0	1	2
3Y-TZP			SS 3		CS 2	
t' (%)			31	37	23	25
t (%)			52	46	52	50
c (%)			14	13	19	19
m (%)			3	4	6	6

3.4. Biaxial flexural strength

3.4.1. Influence of the zirconia on the biaxial flexural strength

3Y-TZP showed the highest BFS, followed by 3/4Y-TZP, while the lowest values were observed for 4Y-TZP. This trend was significant for all 3Y-TZP groups (except SS Layer 3) and the following 3/4Y-TZP groups, HSS Layer 2 and SS Layers 3 and 4, that presented higher values than all 4Y-TZP groups (p < 0.001). 3/4Y-TZP – Layer 1 presented an exception and showed values in a comparable range as 4Y-TZP.

Following CS 1, 3/4Y-TZP showed a lower BFS (p = 0.001) and m in Layer 1, but a higher BFS in Layers 2–4 (p < 0.001) and a higher m in Layer 2 than 4Y-TZP (Table 3).

3.4.2. Influence of the zirconia layer on the biaxial flexural strength

In 3/4Y-TZP, Layers 2–4 showed a higher BFS than Layer 1 (p < 0.001), with Layer 1 presenting a lower m than HSS Layers 2&4, SS Layers 2–4 and CS Layer 2. In SS and CS 3/4Y-TZP, Layer 4 furthermore demonstrated a higher BFS than Layer 2 (p < 0.001).

In 4Y-TZP, HSS Layer 3 (p < 0.019) and SS Layer 2 (p < 0.034) showed a higher BFS than Layer 4. HSS Layer 2 showed a higher m than Layers 1&4, SS Layers 1&2 a higher m than Layers 3&4, and CS Layer 1 a higher m than Layer 3.

In SS 3Y-TZP, Layer 4 showed a higher m than Layers 1–3, while in CS 3Y-TZP, Layer 4 showed a lower m than Layers 1–3.

3.4.3. Influence of the sintering protocol on the biaxial flexural strength

In 3/4Y-TZP – Layers 2&3, HSS and SS led to higher values than CS (p < 0.001). In Layer 2, CS resulted in a higher m than HSS and SS, and in Layer 3, SS led to a higher m than HSS. In Layer 4, SS led to higher values than HSS and CS (p < 0.001).

In 4Y-TZP – Layer 1, SS and CS resulted in a higher m than HSS, while in Layer 2, HSS and SS led to a higher m than CS. In Layer 4, CS led to higher values than SS (p < 0.021).

In 3Y-TZP – Layers 3&4, CS resulted in a higher BFS than SS (p = 0.006–0.008), with SS leading to a higher m than CS in Layer 4.

Reconstruction of broken fragments after BFS testing showed 2 to 6 radial cracks originating from the point of loading.

3.5. Fracture load

3.5.1. Influence of the zirconia on the fracture load

When comparing all groups, 3/4Y-TZP showed the highest FL, followed by 3Y-TZP, while 4Y-TZP showed the lowest values. This tendency was significant for all 3/4Y-TZP groups (except aged HSS 3/4Y-TZP) and non-aged SS 3Y-TZP, that presented higher values than non-aged 4Y-TZP (p < 0.001).

When comparing materials sintered with an identical sintering protocol (namely CS protocol 1), 3/4Y-TZP showed higher FL values than 4Y-TZP (p < 0.001) (Table 4).

3.5.2. Influence of the sintering protocol on the fracture load

For aged 3/4Y-TZP, SS resulted in the highest and HSS in the lowest FL (p = 0.004). For aged 4Y-TZP, HSS led to the highest values (p = 0.005).

3.5.3. Influence of aging on the fracture load

For SS 3/4Y-TZP and HSS 4Y-TZP, aging led to higher FL values than observed initially (p < 0.001–0.012). For HSS 3/4Y-TZP and CS 3Y-TZP, aging resulted in lower m.

Fractures solely originated from a failure in the connector (Fig. 5).

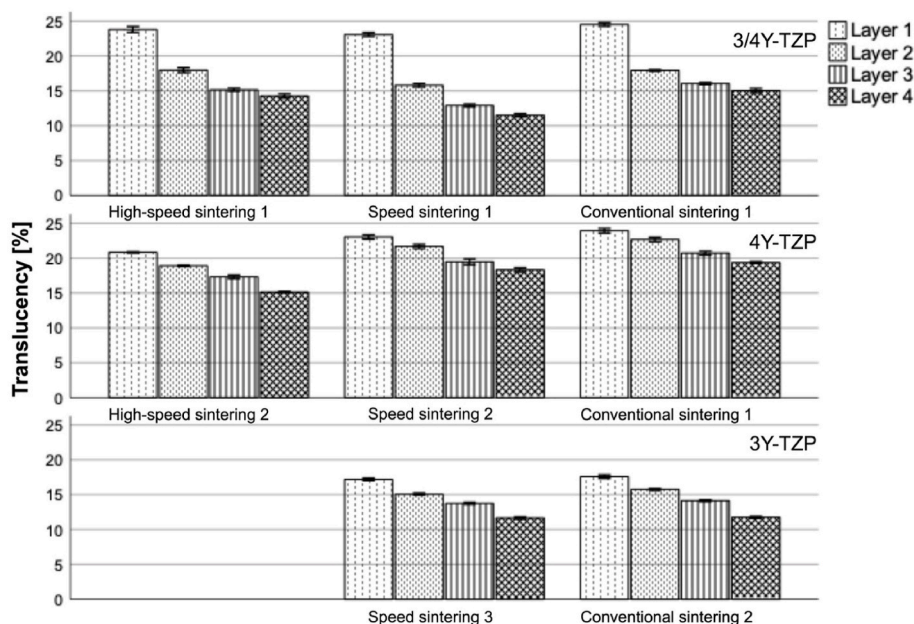


Fig. 4. Bar graphs for the translucency (Mean ± SD) in [%] of the different groups.

**Table 3**  
Descriptive statistics for the biaxial flexural strength *BFS* (Mean ± SD [95% CI]) in [MPa] and the Weibull modulus *m* (Median [95% CI]) of the different groups.

		HSS 1	SS 1	CS 1			
3/4Y-TZP							
Layer 1	<i>BFS</i>	443 ± 130 <sup>Aα</sup>	[349; 536]	559 ± 118 <sup>Aα</sup>	[473; 644]	553 ± 88 <sup>aAα</sup>	[489; 616]
	<i>m</i>	3.6 <sup>Aα</sup>	[1.7; 6.9]	4.9 <sup>Aα</sup>	[2.4; 9.3]	6.8 <sup>aAα</sup>	[3.4; 13.1]
Layer 2	<i>BFS</i>	997 ± 113 <sup>Bβ</sup>	[914; 1078]	945 ± 103 <sup>Bβ</sup>	[871; 1019]	812 ± 46 <sup>bBα</sup>	[778; 846]
	<i>m</i>	9.8 <sup>Bα</sup>	[4.9; 18.7]	10.0 <sup>Bα</sup>	[5.1; 19.3]	20.0 <sup>bbβ</sup>	[10.3; 38.4]
Layer 3	<i>BFS</i>	969 ± 157 <sup>Bβ</sup>	[855; 1082]	1069 ± 86 <sup>BCβ</sup>	[1006; 1131]	824 ± 86 <sup>bBCα</sup>	[761; 886]
	<i>m</i>	6.8 <sup>ABα</sup>	[3.4; 13.1]	14.3 <sup>Bβ</sup>	[7.3; 27.4]	10.8 <sup>aABαβ</sup>	[5.5; 20.8]
Layer 4	<i>BFS</i>	853 ± 103 <sup>Bα</sup>	[778; 926]	1112 ± 80 <sup>Cβ</sup>	[1053; 1170]	932 ± 120 <sup>aBCα</sup>	[845; 1018]
	<i>m</i>	9.0 <sup>Bα</sup>	[4.5; 17.3]	15.7 <sup>Bα</sup>	[8.1; 30.2]	11.2 <sup>aABα</sup>	[5.7; 21.4]
4Y-TZP		HSS 2	SS 2	CS 1			
Layer 1	<i>BFS</i>	628 ± 85 <sup>ABα</sup>	[565; 689]	609 ± 40 <sup>ABα</sup>	[578; 638]	673 ± 45 <sup>bAα</sup>	[639; 705]
	<i>m</i>	8.1 <sup>Aα</sup>	[4.1; 15.6]	16.8 <sup>Bβ</sup>	[8.6; 32.2]	17.5 <sup>bbβ</sup>	[9.0; 33.6]
Layer 2	<i>BFS</i>	637 ± 38 <sup>ABα</sup>	[608; 664]	638 ± 26 <sup>Bα</sup>	[618; 658]	654 ± 83 <sup>aAα</sup>	[593; 715]
	<i>m</i>	18.5 <sup>Bβ</sup>	[9.5; 35.5]	27.6 <sup>Bβ</sup>	[14.2; 52.9]	9.0 <sup>aABα</sup>	[4.6; 17.3]
Layer 3	<i>BFS</i>	659 ± 63 <sup>Bα</sup>	[612; 705]	590 ± 88 <sup>ABα</sup>	[526; 653]	674 ± 91 <sup>aAα</sup>	[608; 740]
	<i>m</i>	11.4 <sup>ABβ</sup>	[5.8; 21.9]	7.5 <sup>Aα</sup>	[3.8; 14.4]	8.4 <sup>aAα</sup>	[4.2; 16.1]
Layer 4	<i>BFS</i>	560 ± 82 <sup>aAαβ</sup>	[499; 619]	548 ± 88 <sup>Aα</sup>	[483; 611]	645 ± 68 <sup>aAβ</sup>	[595; 695]
	<i>m</i>	7.2 <sup>Aα</sup>	[3.6; 13.8]	6.6 <sup>Aα</sup>	[3.3; 12.6]	10.7 <sup>aABα</sup>	[5.4; 20.6]
3Y-TZP			SS 3	CS 2			
Layer 1	<i>BFS</i>		1042 ± 136 <sup>Aα</sup>	[943; 1140]	1083 ± 137 <sup>Aα</sup>		[984; 1182]
	<i>m</i>		8.6 <sup>Aα</sup>	[4.3; 16.5]	8.7 <sup>Bα</sup>		[4.4; 16.7]
Layer 2	<i>BFS</i>		1073 ± 145 <sup>Aα</sup>	[968; 1177]	1192 ± 154 <sup>Aα</sup>		[1081; 1303]
	<i>m</i>		8.2 <sup>Aα</sup>	[4.1; 15.7]	8.8 <sup>Bα</sup>		[4.4; 16.8]
Layer 3	<i>BFS</i>		963 ± 143 <sup>Aα</sup>	[859; 1066]	1172 ± 153 <sup>Aβ</sup>		[1061; 1281]
	<i>m</i>		7.5 <sup>Aα</sup>	[3.8; 14.5]	8.1 <sup>Bα</sup>		[4.1; 15.6]
Layer 4	<i>BFS</i>		986 ± 44 <sup>Aα</sup>	[953; 1018]	1013 ± 297 <sup>aAβ</sup>		[800; 1226]
	<i>m</i>		25.3 <sup>Bβ</sup>	[13.1; 48.5]	2.7 <sup>Aα</sup>		[1.3; 5.3]

\* Not normally distributed.  
abc Different letters present significant differences between materials within one layer and sintering protocol.  
ABC Different letters present significant differences between layers within one material and sintering protocol.  
αβγ Different letters present significant differences between sintering protocols within one material and layer.

3.6. Correlations

A negative correlation between t-phase and *T* ( $R = -0.712, p = 0.002$ ), c + t'-phases and *BFS* ( $R = -0.93, p < 0.001$ ), and *T* and *BFS* ( $R = -0.702, p < 0.001$ ) and a positive correlation between c + t'-phases and *T* ( $R = 0.741, p = 0.001$ ), t-phase and *BFS* ( $R = 0.895, p < 0.001$ ), *BFS* and fracture type ( $R = 0.409, p < 0.001$ ) and *BFS* and *FL* for Layers

2, 3 and 4 was observed ( $R = 0.600-680, p < 0.001$ ) (Fig. 6).

4. Discussion

The tested hypotheses that neither the zirconia, layer nor the sintering protocol presented an impact on the *GS*, crystal phases, *T*, and *BFS* and that the zirconia, sintering protocol and thermomechanical aging did not influence the *FL* of three-unit FDPs were rejected.

4.1. Zirconia

The comparison of the three zirconia showed high optical and low mechanical properties for 4Y-TZP and low optical and high mechanical properties for 3Y-TZP. The strength-gradient multi-layer 3/4Y-TZP showed a varying behavior depending on the examined layer, with Layer 1 showing a comparable *GS* and increased amount of the c + t'-phase as 4Y-TZP, while Layers (2-4) presented smaller grains and a crystal structure comparable to 3Y-TZP. These findings are in line with previous investigations examining 3Y-TZP - and 4Y-TZP (Jerman et al., 2021; Lumkemann and Stawarczyk, 2021). In all materials, *T* declined from Layer 1 to 4, replicating the color gradient of the natural tooth from the translucent incisal edge to the opaquer body, which has already been described for the examined 3/4Y-TZP and 4Y-TZP (Michailova et al., 2020; Inokoshi et al., 2023). 3/4Y-TZP - Layer 1 showed the highest *T*, followed by the 4Y-TZP layers, indicating 3/4Y-TZP - Layer 1 to possess a slightly higher amount of yttrium oxide or less coloring pigments. The lower layers of 3/4Y-TZP and 3Y-TZP behaved similarly. In line with the negative correlation between *T* and *BFS*, 3/4Y-TZP - Layer 1 and 4Y-TZP showed lower *BFS* values surpassed by 3/4Y-TZP Layers 2-4 and 3Y-TZP. The mechanical properties are mirrored in the crystal structure, with 3/4Y-TZP - Layer 4 and 3Y-TZP showing a higher amount of t-phase ( $\geq 40\%$  vs.  $< 30\%$ ). The heightened ability for tetragonal to monoclinic phase transformations can enhance the fracture toughness and explain the improved *BFS* (Belli et al., 2021; Cokic et al., 2022), a theory which is corroborated by the increased amount of m-phase in 3/4Y-TZP - Layer 4 and 3Y-TZP. In accordance with the described relationships between the crystal structure and the optical and mechanical properties of zirconia, the t-phase showed a positive correlation to *BFS*, while the c + t'-phase correlated with *T*. As seen, e.g., in the comparison of 3Y-TZP with 4Y-TZP, an increase in the t-phase entails a decrease in the c + t'-phases.

When regarding the different layers within one material, 3/4Y-TZP - Layers 2-4 showed a higher *BFS* than Layer 1. A similar trend was observed for biaxial and 4-point flexural strength (Inokoshi et al., 2023). The 3/4Y-TZP blank thus seems to consist of 4Y-TZP in the upper 35%, a finding supported by the higher amount of c-phase in Layer 1, and color-gradient 3Y-TZP in the bottom 65%. Following SS and CS, Layer 4 demonstrated a higher *BFS* than Layer 2, which may be caused by transition zones arising during the manufacturing of strength-gradient multi-layer blanks. This highly relevant clinical finding underlines the importance of nesting in strength-gradient multi-layer blanks, as this step directly impacts the restorations' optical and mechanical properties (Winter et al., 2022; Strasser et al., 2023). A previous investigation examining the impact of nesting on the *FL* of 5/3Y-TZP FDPs reported higher values for a central positioning of the restoration in comparison with nesting at the top or bottom of the blank (Rosentritt et al., 2022).

The connection between *T* and *BFS* did not hold for 4Y-TZP, where solely HSS Layer 3 and SS Layer 2 showed a higher *BFS* than Layer 4, and 3Y-TZP, where no differences were observed between the layers. For the multi-color 3Y-TZP and 4Y-TZP, *T* is configured by a varying doting with pigments. As observed for most groups, the mechanical properties defined by the *GS* and crystal structure should be stable throughout the layers. With the different zones of a blank being subject to various pressures during manufacturing, properties may, however, vary. This could be the reason why in 4Y-TZP centrally located HSS Layer 3 and SS Layer 2 showed higher *BFS* values than Layer 4 and why the crystal

**Table 4**

Descriptive statistics for the fracture load *FL* (Mean ± SD [95% CI]) in [N] and the Weibull modulus *m* (Median [95% CI]) of the different groups.

3/4Y-TZP		HSS 1		SS 1		CS 1	
No artificial aging	<i>FL</i>	1459 ± 205 <sup>Aα</sup>	[1311; 1606]	1433 ± 302 <sup>Aα</sup>	[1215; 1649]	1493 ± 346 <sup>B4α</sup>	[1244; 1741]
	<i>m</i>	7.9 <sup>Aβ</sup>	[4.0; 15.2]	5.1 <sup>Aα</sup>	[2.5; 9.7]	4.4 <sup>A4α</sup>	[2.1; 8.4]
Thermo-mechanical aging	<i>FL</i>	1229 ± 423 <sup>Aα</sup>	[903; 1555]	1865 ± 387 <sup>Bβ</sup>	[1586; 2142]	1444 ± 325 <sup>B4Bα</sup>	[1210; 1677]
	<i>m</i>	3.5 <sup>Aα</sup>	[1.5; 6.7]	5.5 <sup>Aα</sup>	[2.7; 10.5]	4.6 <sup>A4α</sup>	[2.3; 8.9]
4Y-TZP		HSS 2		SS 2		CS 1	
No artificial aging	<i>FL</i>	767 ± 136 <sup>Aα</sup>	[668; 864]	758 ± 190 <sup>Aα</sup>	[620; 894]	783 ± 126 <sup>A4α</sup>	[684; 880]
	<i>m</i>	6.4 <sup>Aα</sup>	[3.2; 12.2]	4.7 <sup>Aα</sup>	[2.3; 9.0]	6.7 <sup>A4α</sup>	[3.2; 13.3]
Thermo-mechanical aging	<i>FL</i>	1079 ± 202 <sup>Bβ</sup>	[932; 1224]	830 ± 214 <sup>Aα</sup>	[676; 984]	805 ± 132 <sup>A4α</sup>	[709; 900]
	<i>m</i>	6.3 <sup>Aα</sup>	[3.1; 12.0]	4.2 <sup>Aα</sup>	[2.1; 8.2]	6.4 <sup>A4α</sup>	[3.2; 12.3]
3Y-TZP		SS 3		CS 2		CS 2	
No artificial aging	<i>FL</i>			1441 ± 343 <sup>Aα</sup>	[1194; 1687]	1294 ± 210 <sup>Aα</sup>	[1142; 1445]
	<i>m</i>			4.5 <sup>Aα</sup>	[2.2; 8.7]	7.9 <sup>Aβ</sup>	[4.0; 15.1]
Thermo-mechanical aging	<i>FL</i>			1393 ± 302 <sup>Aα</sup>	[1176; 1610]	1303 ± 384 <sup>Aα</sup>	[1027; 1579]
	<i>m</i>			5.7 <sup>Aα</sup>	[2.8; 11.0]	3.7 <sup>Aα</sup>	[1.8; 7.1]

abc Different letters present significant differences between materials within one sintering protocol and aging level.  
 ABC Different letters present significant differences between sintering protocols within one material and aging level.  
 αβγ Different letters present significant differences between aging levels within one material and sintering protocol.



Fig. 5. A fractured FDP, with the failure originating from the connector.

structure of 4Y-TZP and 3Y-TZP showed some variations in the amount of c-phase between Layers 1 and 4.

As previously described (Quinn, 2020), the analyses showed a positive correlation between *BFS* and the number of radial cracks. For most groups, materials with a higher homogeneity, quantified by *m*, also presented a higher *BFS*. As this trend was not exempt from exceptions, future studies are warranted to i. a. investigate the influence of coloring on the reliability of zirconia, with previous studies reporting both no impact and a negative effect on the mechanical properties (Sedda et al., 2015; Pittayachawan et al., 2007; Liu et al., 2010).

3/4Y-TZP showed the highest *FL*, followed by 3Y-TZP, while 4Y-TZP presented the lowest values. This finding is corroborated by an investigation of anterior three-unit FDPs reporting 3/4Y-TZP to result in similar *FL* as 3Y-TZP, while 4Y-TZP led to lower results (Poppel et al., 2022). With fractures solely originating from the connector (Poppel et al., 2022; Zacher et al., 2020), nested in Layers 2&3 and the uppermost part of Layer 4, and a correlation between *FL* and *BFS* in Layers 1–4 being found, the low mechanical properties of 3/4Y-TZP's Layer 1 do not seem to carry weight. This finding underscores the principle of using strength-gradient multi-layer blanks to profit from high optical properties in the incisal area, while ensuring high mechanical properties in the lower areas subject to tensile forces. A fractographic analysis of 3/4Y-TZP showed the crack pattern to be independent of the interface, implying that these do not form a weak link in strength-gradient multi-layered zirconia (Inokoshi et al., 2023).

#### 4.2. Sintering protocol

In 3/4Y-TZP, CS resulted in the highest *T*, and was followed by or equal to HSS, while SS led to the lowest values. In Figure A4, the many times larger AUC of CS compared with HSS and SS is apparent. The larger enthalpy transfer forms larger grains in CS 3/4Y-TZP (Stawarczyk et al., 2014; Attia et al., 2023). The lower number of grain boundaries and grain boundary pores decreases light reflections and refractions, and results in an increased *T*. Despite its lower AUC, the higher heating rate and firing temperature during HSS resulted in the formation of larger grains than SS, which may visualize the increased c- and t'-phase, resulting in a reduced optical birefringence and in consequence, higher *T* (Stawarczyk et al., 2014).

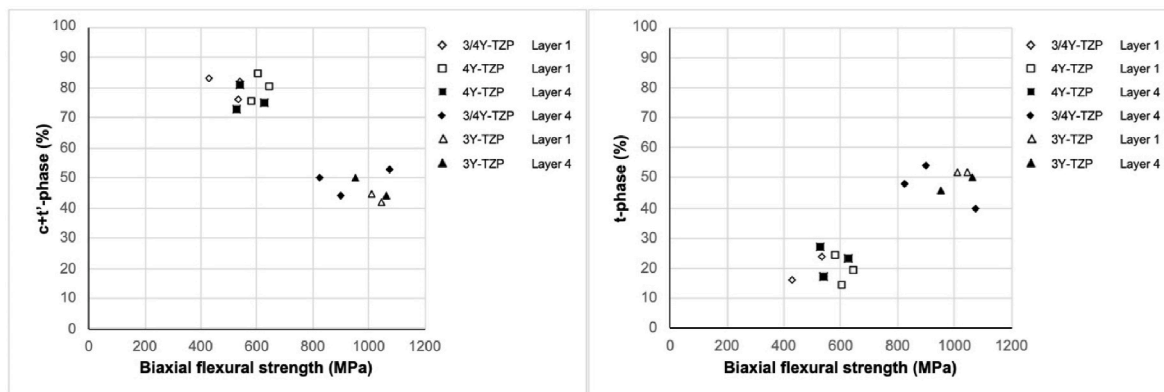


Fig. 6. Scatter plots showing the correlation between c + t'-phases and *BFS*, and t-phase and *BFS*.

Whilst a close connection between optical and mechanical properties has been reported for 3Y-TZPs (Camposilvan et al., 2018; Stawarczyk et al., 2013), the sintering conditions may exercise a more direct impact on the optical properties of 4Y-TZP than on its mechanical behavior. This hypothesis is supported by this analysis showing no influence of the sintering conditions on the *BFS* of 3/4Y-TZP – Layer 1. Hence, CS should be employed to achieve the highest optical properties for 4Y-TZP, while HSS convinces with its much shorter sintering duration. With SS presenting the lowest *T*, this sintering protocol does not demonstrate an advantage.

In 3/4Y-TZP – Layers 2–4, CS resulted in low and SS in high *BFS* values. In line with the negative correlation observed between *T* and *BFS*, the mechanical properties of the zirconia thus behaved contrarily to the reported optical properties (Stawarczyk et al., 2013). The reduced resistance against loading is related to the larger *GS* in the CS zirconia. The smaller grains seen after SS may limit the size of dislocations on the grain boundaries, requiring a higher stress to induce permanent material deformations (Palmero, 2015; Pereira et al., 2018). CS led to a higher reliability in Layer 2 than HSS and SS, which is underlined by the more even distribution of grains. Interestingly, SS led to a higher *m* than HSS in Layer 3. For HSS, SEM showed exceedingly large grains interspersed with small grains, hinting at this stark inhomogeneity to result in a reduced reliability. In conclusion, sintering of 3Y-TZP requires a balancing act between the optical properties on one side, and the mechanical properties and the required time on the other. With HSS showing varying results between those of CS and SS despite its short duration, it may be able to strike this balance best. With fractures originating from the bottom of the connectors, which are subjected to the maximum tensile forces, *FL* should in theory only depend on Layers 3&4 (Zacher et al., 2020). While a previous investigation examining the 3/4Y-TZP reported the highest *FL* after HSS, followed by SS and then CS (Attia et al., 2023), initially no differences in *FL* were observed between the sintering protocols, hinting to a reduced importance of the sintering parameters when regarding multi-unit FDPs. After aging, SS showed higher *FL* than reported initially and thereby differentiated itself from HSS. These findings partly mirror those observed for *BFS* in Layer 4.

In 4Y-TZP, CS resulted in the highest *T*, followed by SS, while HSS led to the lowest. This finding can be traced regarding the AUCs and is mirrored in the *GS* (Liu et al., 2022b). As for 3/4Y-TZP – Layer 1, the sintering protocol did not impact the mechanical properties of 4Y-TZP, except in Layer 4, where CS resulted in higher values than SS. The higher amount of t-phase following CS entails a higher ability for tetragonal to monoclinic phase transformations and could translate into a higher *BFS*. The uniform grains for CS may surpass the properties achieved by the variation of smaller and excessively large grains formed by the higher heating rate in SS. While no differences were observed between the sintering protocols initially, aged HSS 4Y-TZP showed higher *FL* than the other two groups. This finding, which is not reflected in *BFS*, may be related to the higher resistance of the smaller HSS grains to dislocations during aging (Palmero, 2015; Pereira et al., 2018). As a result of the disparate outcome for *T/BFS* (favoring CS) and *FL* (favoring HSS), a final assessment of the sintering protocols for 4Y-TZP is not feasible.

In 3Y-TZP, CS led to a higher *T* in Layers 1–3, a higher *GS* and a higher *BFS* in Layers 3&4 than SS, and thus represents the sintering protocol of choice. While the findings for the optical behavior of the zirconia are supported by its *GS* (which can be traced to the AUCs) and the higher amount of c-phase after CS, the conformity in the optical and mechanical behavior of 3Y-TZP in Layers 3&4 is surprising, with the majority of previous investigations reporting a negative correlation (Camposilvan et al., 2018; Stawarczyk et al., 2013) and only one investigation a positive correlation between these properties (Lumke-mann et al., 2020). Although SS led to smaller less evenly distributed grains, it presented a higher reliability than CS in Layer 4. The heterogenous structure may increase the ability to deflect micro cracks and dissipate crack energy, resulting in increased mechanical properties.

#### 4.3. Thermomechanical aging

Aging led to higher *FL* for 2/8 groups (speed sintered 3/4Y-TZP, high-speed sintered 4Y-TZP). The increased amount of c + t'-phase should render 4Y-TZP to be less susceptible to aging than 3/4Y-TZP and 3Y-TZP. The improved strength may be caused by the formation of a compressive layer that reduces the stress-intensity factor and/or enforces tetragonal to monoclinic phase transformations, that lead to tip blunting for present defects (Camposilvan et al., 2018; Marro and Anglada, 2012). For high-speed sintered 3/4Y-TZP and conventionally sintered 3Y-TZP, aging resulted in a lower *m*. Previously existing microcracks and pores may have been exacerbated and new flaws developed during aging, acting as stress concentration sites, and resulting in a lower homogeneity between specimens (Siarampi et al., 2014). With 6000 thermal and 1,200,000 masticatory cycles imitating a clinical situation after 5 years (Rosentritt et al., 2009), this finding indicates a promising long-term behavior for all examined zirconia and sintering protocols. With all groups exceeding the maximum bite forces reported in the posterior region (van der Bilt et al., 2008), the FDPs show sufficient mechanical properties to withstand masticatory forces.

#### 4.4. Limitations

Previous studies reported a higher Y<sub>2</sub>O<sub>3</sub> mol% content of 3.9/5.6 (Inokoshi et al., 2023) for what here was denoted as 3/4Y-TZP, 4.8 (Inokoshi et al., 2018), 5.4 (Lubauer et al., 2023) or 5.8 (Shishido et al., 2023) for 4Y-TZP, and 4.0 (Inokoshi et al., 2018) for KATANA Zirconia HT, Kuraray Noritake Dental, which is the monolayer equivalent to the examined 3Y-TZP, warranting a reevaluation of the denotation of different zirconia. The results of the XRD analyses may have been affected by phase transformations, as analyses were performed after *BFS* measurements.

### 5. Conclusions

Within the limitations of this investigation, the following conclusions can be drawn:

1. A comparison of the 3 zirconia materials showed a higher amount of c- and t'-phase and a lower amount of t-phase, as well as higher optical and lower mechanical properties for 4Y-TZP. Conversely, a lower amount of c- and t'-phase and a higher amount of t-phase, as well as lower optical and higher mechanical properties were observed for 3Y-TZP. *T* and *BFS* showed a negative correlation, while the c + t'-phases and *T*, and the t-phase and *BFS* showed a positive correlation. The behavior of the strength-gradient 3/4Y-TZP suggest Layer 1 to consist of 4Y-TZP and Layers 2–3 of color-gradient 3Y-TZP. In all examined materials, *T* declined from Layer 1 to 4. 3/4Y-TZP showed the highest *FL*, followed by 3Y-TZP, while 4Y-TZP showed the lowest values, underscoring the use of strength-gradient multi-layer blanks to profit from high optical properties in the incisal area, while ensuring high mechanical properties in the lower areas subject to tensile forces.
2. In 4Y-TZP, the sintering parameters exercised a direct impact on the grain size and the optical properties, while the mechanical properties were largely unaffected. The impact of the sintering parameters on 3Y-TZP showed contradictory results, with 3/4Y-TZP - Layers 2–4 presenting diametric optical and mechanical properties in dependence of the sintering protocol, while a conformity in the examined properties was observed for 3Y-TZP Layers 3&4.
3. Thermomechanical aging resulted in comparable or higher *FL*. With all groups exceeding maximum bite forces, the three-unit FDPs showed promising long-term mechanical properties.

## Funding

This research did not receive any specific grant from funding agencies in the public, commercial, or not-for-profit sectors.

## CRedit authorship contribution statement

**Felicitas Mayinger:** Writing – review & editing, Writing – original draft, Visualization, Methodology, Investigation, Formal analysis, Data curation, Conceptualization. **Andreas Ender:** Writing – review & editing, Software, Methodology, Investigation, Conceptualization. **Monika Strickstroock:** Writing – review & editing, Visualization, Methodology, Investigation. **Adham Elsayed:** Writing – review & editing, Conceptualization. **Parissa Nassary Zadeh:** Writing – review & editing, Investigation. **Marcus Zimmermann:** Writing – review & editing, Visualization. **Bogna Stawarczyk:** Writing – review & editing, Project administration, Methodology, Formal analysis, Conceptualization.

## Declaration of competing interest

The authors declare that they have no known competing financial interests or personal relationships that could have appeared to influence the work reported in this paper.

## Data availability

Data will be made available on request.

## Acknowledgements

The authors would like to thank Kuraray Noritake Dental for supporting this study.

## Appendix A. Supplementary data

Supplementary data to this article can be found online at <https://doi.org/10.1016/j.jmbbm.2024.106580>.

## References

- Attia, M.A., Radwan, M., Blunt, L., Bills, P., Tawfik, A., Arafa, A.M., 2023. Effect of different sintering protocols on the fracture strength of 3-unit monolithic gradient zirconia fixed partial dentures: an in vitro study. *J. Prosthet. Dent* 130, 908 e1–e8.
- Belli, R., Hurle, K., Schürlein, J., Petschelt, A., Werbach, K., Peterlik, H., Rabe, T., Mieller, B., Lohbauer, U., 2021. Relationships between fracture toughness, Y2O3 fraction and phases content in modern dental Yttria-doped zirconias. *J. Eur. Ceram. Soc.* 41, 7771–7782.
- Butikofer, L., Stawarczyk, B., Roos, M., 2015. Two regression methods for estimation of a two-parameter Weibull distribution for reliability of dental materials. *Dent. Mater.* 31, e33–e50.
- Composilvan, E., Leone, R., Gremillard, L., Sorrentino, R., Zarone, F., Ferrari, M., Chevalier, J., 2018. Aging resistance, mechanical properties and translucency of different yttria-stabilized zirconia ceramics for monolithic dental crown applications. *Dent. Mater.* 34, 879–890.
- Cokic, S.M., Condor, M., Vleugels, J., Meerbeek, B.V., Oosterwyck, H.V., Inokoshi, M., Zhang, F., 2022. Mechanical properties-translucency-microstructure relationships in commercial monolayer and multilayer monolithic zirconia ceramics. *Dent. Mater.* 38, 797–810.
- Hannink, R.H.J.K.P., Muddle, B.C., 2000. Transformation toughening in zirconia-containing ceramics. *J. Am. Ceram. Soc.* 83 (3), 461–487.
- Inokoshi, M., Shimizu, H., Nozaki, K., Takagaki, T., Yoshihara, K., Nagaoka, N., Zhang, F., Vleugels, J., Van Meerbeek, B., Minakuchi, S., 2018. Crystallographic and morphological analysis of sandblasted highly translucent dental zirconia. *Dent. Mater.* 34, 508–518.
- Inokoshi, M., Liu, H., Yoshihara, K., Yamamoto, M., Tonprasong, W., Benino, Y., Minakuchi, S., Vleugels, J., Van Meerbeek, B., Zhang, F., 2023. Layer characteristics in strength-gradient multilayered yttria-stabilized zirconia. *Dent. Mater.* 39, 430–441.
- Jansen, J.U., Lumkemann, N., Letz, I., Pfefferle, R., Sener, B., Stawarczyk, B., 2019. Impact of high-speed sintering on translucency, phase content, grain sizes, and flexural strength of 3Y-TZP and 4Y-TZP zirconia materials. *J. Prosthet. Dent* 122, 396–403.
- Jerman, E., Wiedenmann, F., Eichberger, M., Reichert, A., Stawarczyk, B., 2020. Effect of high-speed sintering on the flexural strength of hydrothermal and thermo-mechanically aged zirconia materials. *Dent. Mater.* 36, 1144–1150.
- Jerman, E., Lumkemann, N., Eichberger, M., Zoller, C., Nothelfer, S., Kienle, A., Stawarczyk, B., 2021. Evaluation of translucency, Marten's hardness, biaxial flexural strength and fracture toughness of 3Y-TZP, 4Y-TZP and 5Y-TZP materials. *Dent. Mater.* 37, 212–222.
- Kaizer, M.R., Gierthmuehlen, P.C., Dos Santos, M.B., Cava, S.S., Zhang, Y., 2017. Speed sintering translucent zirconia for chairside one-visit dental restorations: optical, mechanical, and wear characteristics. *Ceram. Int.* 43, 10999–11005.
- Kolakarprasert, N., Kaizer, M.R., Kim, D.K., Zhang, Y., 2019. New multi-layered zirconias: composition, microstructure and translucency. *Dent. Mater.* 35, 797–806.
- Liu, Q., Shao, L.Q., Wen, N., Deng, B., 2010. Surface microhardness and flexural strength of colored zirconia. *AMR (Adv. Magn. Reson.)* 105–106, 49–50.
- Liu, Y.C., Lin, T.H., Lin, Y.Y., Hu, S.W., Liu, J.F., Yang, C.C., Yan, M., 2022a. Optical properties evaluation of rapid sintered translucent zirconia with two dental colorimeters. *J. Dent. Sci.* 17, 155–161.
- Liu, H., Inokoshi, M., Nozaki, K., Shimizubata, M., Nakai, H., Cho Too, T.D., Minakuchi, S., 2022b. Influence of high-speed sintering protocols on translucency, mechanical properties, microstructure, crystallography, and low-temperature degradation of highly translucent zirconia. *Dent. Mater.* 38, 451–468.
- Lubauer, J., Schuenemann, F.H., Belli, R., Lohbauer, U., 2023. Speed-sintering and the mechanical properties of 3-5 mol% Y(2)O(3)-stabilized zirconias. *Odontology* 111, 883–890.
- Lumkemann, N., Stawarczyk, B., 2021. Impact of hydrothermal aging on the light transmittance and flexural strength of colored yttria-stabilized zirconia materials of different formulations. *J. Prosthet. Dent* 125, 518–526.
- Lumkemann, N., Pfefferle, R., Jerman, E., Sener, B., Stawarczyk, B., 2020. Translucency, flexural strength, fracture toughness, fracture load of 3-unit FDPs, Martens hardness parameter and grain size of 3Y-TZP materials. *Dent. Mater.* 36, 838–845.
- Marro, F.G., Anglada, M., 2012. Strengthening of Vickers indented 3Y-TZP by hydrothermal ageing. *J. Eur. Ceram. Soc.* 32, 317–324.
- Michailova, M., Elsayed, A., Fabel, G., Edelhoff, D., Zylla, I.M., Stawarczyk, B., 2020. Comparison between novel strength-gradient and color-gradient multilayered zirconia using conventional and high-speed sintering. *J. Mech. Behav. Biomed. Mater.* 111, 103977.
- Nassary Zadeh, P., Lumkemann, N., Sener, B., Eichberger, M., Stawarczyk, B., 2018. Flexural strength, fracture toughness, and translucency of cubic/tetragonal zirconia materials. *J. Prosthet. Dent* 120, 948–954.
- Palmero, P., 2015. Structural ceramic nanocomposites: a review of properties and powders' synthesis methods. *Nanomaterials (Basel)* 5, 656–696.
- Pereira, G.K.R., Guillard, L.F., Dapieve, K.S., Kleverlaan, C.J., Rippe, M.P., Valandro, L.F., 2018. Mechanical reliability, fatigue strength and survival analysis of new polycrystalline translucent zirconia ceramics for monolithic restorations. *J. Mech. Behav. Biomed. Mater.* 85, 57–65.
- Pittayachawan, P., McDonald, A., Petrie, A., Knowles, J.C., 2007. The biaxial flexural strength and fatigue property of Lava Y-TZP dental ceramic. *Dent. Mater.* 23, 1018–1029.
- Poppel, M.L., Rosentritt, M., Sturm, R., Beuer, F., Hey, J., Schmid, A., Schmidt, F., 2022. Fracture load and fracture patterns of monolithic three-unit anterior fixed dental prostheses after in vitro artificial aging-A comparison between color-gradient and strength-gradient multilayer zirconia materials with varying yttria content. *J. Clin. Med.* 11 (17), 4982.
- Quinn, G., 2020. NIST recommended practice guide. *Fractography of Ceramics and Glasses*, third ed. <https://doi.org/10.6028/NIST.SP.960-16e3>
- Rosentritt, M., Behr, M., van der Zel, J.M., Feilzer, A.J., 2009. Approach for valuating the influence of laboratory simulation. *Dent. Mater.* 25, 348–352.
- Rosentritt, M., Behr, M., Scharnagl, P., Handel, G., Kolbeck, C., 2011. Influence of resilient support of abutment teeth on fracture resistance of all-ceramic fixed partial dentures: an in vitro study. *Int. J. Prosthodont.* (IJP) 24, 465–468.
- Rosentritt, M., Preis, V., Behr, M., Strasser, T., 2020. Fatigue and wear behaviour of zirconia materials. *J. Mech. Behav. Biomed. Mater.* 110, 103970.
- Rosentritt, M., Preis, V., Schmid, A., Strasser, T., 2022. Multilayer zirconia: influence of positioning within blank and sintering conditions on the in vitro performance of 3-unit fixed partial dentures. *J. Prosthet. Dent* 127, 141–145.
- Sedda, M., Vichi, A., Carrabba, M., Capperucci, A., Louca, C., Ferrari, M., 2015. Influence of coloring procedure on flexural resistance of zirconia blocks. *J. Prosthet. Dent* 114, 98–102.
- Shishido, S., Inagaki, R., Kanno, T., Svanborg, P., Barkarmo, S., Ortengren, U., Nakamura, K., 2023. Residual stress associated with crystalline phase transformation of 3-6 mol% yttria-stabilized zirconia ceramics induced by mechanical surface treatments. *J. Mech. Behav. Biomed. Mater.* 146, 106067.
- Siarampi, E., Kontonasaki, E., Andrikopoulos, K.S., Kantiranis, N., Voyiatzis, G.A., Zorba, T., Paraskevopoulos, K.M., Koidis, P., 2014. Effect of in vitro aging on the flexural strength and probability to fracture of Y-TZP zirconia ceramics for all-ceramic restorations. *Dent. Mater.* 30, e306–e316.
- Stawarczyk, B., Ozcan, M., Trottmann, A., Hammerle, C.H., Roos, M., 2012. Evaluation of flexural strength of hiped and presintered zirconia using different estimation methods of Weibull statistics. *J. Mech. Behav. Biomed. Mater.* 10, 227–234.
- Stawarczyk, B., Ozcan, M., Hallmann, L., Ender, A., Mehl, A., Hammerle, C.H., 2013. The effect of zirconia sintering temperature on flexural strength, grain size, and contrast ratio. *Clin. Oral Invest.* 17, 269–274.
- Stawarczyk, B., Emslander, A., Roos, M., Sener, B., Noack, F., Keul, C., 2014. Zirconia ceramics, their contrast ratio and grain size depending on sintering parameters. *Dent. Mater.* J. 33, 591–598.

- Stawarczyk, B., Frevert, K., Ender, A., Roos, M., Sener, B., Wimmer, T., 2016. Comparison of four monolithic zirconia materials with conventional ones: contrast ratio, grain size, four-point flexural strength and two-body wear. *J. Mech. Behav. Biomed. Mater.* 59, 128–138.
- Strasser, T., Wertz, M., Koenig, A., Koetzsche, T., Rosentritt, M., 2023. Microstructure, composition, and flexural strength of different layers within zirconia materials with strength gradient. *Dent. Mater.* 39, 463–468.
- Technical Committee ISO/TC 106/SC 2, International Organization for Standardization, 2015. *Dentistry – Ceramic Materials. ISO 6872: 2015*.
- van der Bilt, A., Tekamp, A., van der Glas, H., Abbink, J., 2008. Bite force and electromyography during maximum unilateral and bilateral clenching. *Eur. J. Oral Sci.* 116, 217–222.
- Wertz, M., Fuchs, F., Hoelzig, H., Wertz, J.M., Kloess, G., Hahnel, S., Rosentritt, M., Koenig, A., 2021. The influence of surface preparation, chewing simulation, and thermal cycling on the phase composition of dental zirconia. *Materials* 14, 2133.
- Winter, A., Schurig, A., Odenthal, A.-L., Schmitter, M., 2022. Impact of different layers within a blank on mechanical properties of multi-layered zirconia ceramics before and after thermal aging. *Dent. Mater.* 38, e147–e154.
- Zacher, J., Bauer, R., Strasser, T., Rosentritt, M., 2020. Laboratory performance and fracture resistance of CAD/CAM implant-supported tooth-coloured anterior FDPs. *J. Dent.* 96, 103326.
- Zhang, F., Inokoshi, M., Batuk, M., Hadermann, J., Naert, I., Van Meerbeek, B., Vleugels, J., 2016. Strength, toughness and aging stability of highly-translucent Y-TZP ceramics for dental restorations. *Dent. Mater.* 32, e327–e337.